Transformed cells after senescence give rise to more severe tumor phenotypes than transformed non-senescent cells

Alberta Palazzo, Hector Hernandez-Vargas, Delphine Goehrig, Jean-Jacques Médard, David Vindrieux, Jean-Michel Flaman, David Bernard

▶ **To cite this version:**

Alberta Palazzo, Hector Hernandez-Vargas, Delphine Goehrig, Jean-Jacques Médard, David Vindrieux, et al.. Transformed cells after senescence give rise to more severe tumor phenotypes than transformed non-senescent cells. Cancer Letters, 2022, 546, pp.215850. 10.1016/j.canlet.2022.215850 . hal-03854769

HAL Id: hal-03854769
https://hal.science/hal-03854769v1

Submitted on 23 Aug 2023

HAL is a multi-disciplinary open access archive for the deposit and dissemination of scientific research documents, whether they are published or not. The documents may come from teaching and research institutions in France or abroad, or from public or private research centers.

L'archive ouverte pluridisciplinaire **HAL**, est destinée au dépôt et à la diffusion de documents scientifiques de niveau recherche, publiés ou non, émanant des établissements d'enseignement et de recherche français ou étrangers, des laboratoires publics ou privés.

Transformed cells after senescence give rise to more severe tumor phenotypes than transformed non-senescent cells

Alberta Palazzo[a], Hector Hernandez-Vargas[a], Delphine Goehrig[a], Jean-Jacques Médard[a], David Vindrieux[a], Jean-Michel Flaman[a,*], David Bernard[a,*]

[a]Centre de Recherche en Cancérologie de Lyon, Inserm U1052, CNRS UMR 5286, Centre Léon Bérard, Université de Lyon, Lyon, France

*shared senior co-authorship

Corresponding authors: jean-michel.flaman@lyon.unicancer.fr;

david.bernard@lyon.unicancer.fr

Abstract

Oncogenic stress-induced senescence initially inhibits tumor initiation by blocking proliferation and by attracting immune cells to clear potentially harmful cells. If these cells are not eliminated they may resume proliferation upon loss-of-tumor suppressors, and be at risk of transformation. During tumor formation, depending on the sequence of events of gain-of-oncogenes and/or loss-of-tumor suppressors, cancer cells may emerge from senescent cells. Here, we show that these transformed cells after senescence (TS) display more aggressive tumorigenic features, with a greater capacity to migrate and a higher resistance to anti-tumoral drugs than cells having undergone transformation without senescence. Bulk transcriptomic analysis and single cell RNA sequencing revealed a signature unique to TS cells. A score of this signature was then generated and a high score was correlated with decreased survival of patients with lung adenocarcinoma, head-neck squamous cell carcinoma, adrenocortical carcinoma, liver hepatocellular carcinoma, skin cutaneous melanoma and low-grade glioma. Together, these findings strongly support that cancer cells arising from senescent cells are more dangerous, and that a molecular signature of these cells may be of prognostic value for some human cancers. It also raises questions about modeling human tumors, using cells or mice, without regards to the sequence of events leading to transformation.

Keywords: Cellular senescence, RAS oncogene, p53 tumor suppressor, tumor aggressiveness

1. Introduction

Cellular senescence is characterized by a stable cell cycle arrest and a senescence-associated secretory program (SASP), which entails the release by these cells of inflammatory factors, growth factors and metalloproteases, involved in the pathophysiological effects of senescent cells [1,2].

Cellular senescence when induced by oncogenic stress, named oncogene-induced senescence (OIS), for instance, initially blocks tumorigenesis by inhibiting cell proliferation and by inducing the clearance of these harmful and altered cells by immune cells attracted by their SASP. In the event of escape from senescence either by inactivation of tumor suppressor genes, such as p53 or p16 [3-5], or by failure of the immune surveillance [6], transformation may be initiated and progress. In addition, emerging evidence shows that accumulation of senescent cells, which occurs during aging, after oncogenic activation, or upon exposure to environmental chronic stresses, may trigger tumor formation and progression. Such modifications include suppressing the immune surveillance activity and/or fostering genetic instability and the epithelial-to-mesenchymal transition (EMT), which enhances migratory and invasive phenotypes, reprogramming and stemness [7-14].

Senescent cells, in particular those arising in response to an oncogenic stress, which are not eliminated by the organism, may have the capacity to resume growth if key pathways involved in sustaining proliferation arrest are altered, for instance via p53 loss-of-function [3-5]. The properties and behaviors of such cells compared to cells having undergone transformation without entering senescence are currently unknown.

Here, we modeled cell transformation using mouse embryonic fibroblasts (MEFs) subjected to an inverse sequence of events: i) gain-of-RasV12 oncogene and loss-of-p53 tumor suppressor, leading to transformed cells after senescence (TS), or ii) the opposite, resulting in transformed (T) non-senescent cells. Our data support that the sequence of events leading to

cell transformation strongly impacts the phenotype of transformed cells, with TS cells being more prone to forming tumors and to displaying aggressive and resistant phenotypes. In addition, by crossing bulk and single cell RNA sequencing data, we identified a molecular signature of such transformed cells after senescence which is correlated with poorer patient prognosis for some human cancers.

2. Materials and methods

2.1. Cell culture

Mouse embryonic fibroblasts (MEFs) were isolated from E12.5-E13.5 embryos from pregnant C57BL/6 mice, and cultured in high glucose Dulbecco's Modified Eagle's Medium with GlutaMax, (DMEM, Life Technologies, Carlsbad, USA) supplemented with 10% fetal bovine serum (FBS) (Sigma-Aldrich, Saint-Louis, USA), 1% penicillin-streptomycin (Life Technologies) and 1% MEM non-essential amino acid (Gibco™). Virus-producing cells 293T and Plat-E (Clontech, Mountain View, CA, USA) were cultured in DMEM containing GlutaMAX and supplemented with 10% FBS and 1% penicillin-streptomycin. Cells were maintained at 37°C under a 5% CO_2 atmosphere.

2.2. Plasmids and virus production

For virus production, 293T and Plat-E cells were transfected using GeneJuice reagent according to the manufacturer's recommendations (Merck Millipore). Briefly for lentiviral production, 293T cells were transfected with pSicoRp53 (Addgene plasmid #12090), encoding short hairpin RNA (shRNA) against Trp53 and helper vectors pCMVdeltaR8.91 and phCMVG. For retroviral production, Plat-E cells were transfected with pBABE-puro-H-RasV12 vector (Addgene plasmid #9051), encoding an oncogenic form of RasV12. In parallel, infection with control vectors, pSicoR (Addgene plasmid #11579), pBABE-puro (Addgene plasmid #1764) and pLPC/GFP (Addgene plasmid #65436), were performed to check that infections *per se* had no effect or to verify the percentage of infected cells by monitoring to GFP signal (> 90%) (data not shown).

Seventy-two hours after transfection, viral supernatants were harvested, centrifuged at 160*g* for 5 min and filtered through a 0.45 µm pore size filter. The supernatants were then combined with fresh medium (1/10 for lentivirus and 1/5 for retrovirus) supplemented with 8

µg/mL hexadimethrine bromide (SigmaAldrich) and added to targeted cells for 8 h.

2.3. Senescence-associated β-galactosidase and crystal violet assays

For senescence-associated activity of β-galactosidase (SA-β-Galactosidase), cells were washed with PBS, fixed for 15 min in 0.5% glutaraldehyde, rinsed twice in PBS 1X, and incubated at 37°C for 6 to 12 hr in SA-β-Galactosidase staining solution as previously described [15]. For crystal violet assay, cells were washed with PBS, fixed for 15 min in 3.7% formaldehyde and stained with crystal violet solution.

2.4. Growth curves

Three thousand cells were seeded in 10 cm in diameter dishes at the start of the growth curve. Cells were counted and 240,000 cells were seeded at each passage. Population doubling (PD) was calculated according to the following formula: $PD = \ln(N/N_0)/\ln 2$. N represents the number of counted cells and N_0 the number of seeded cells.

2.5. Anti-tumor drug assay

In a 12-well plate, 20,000 cells were seeded per well and treated twice (day 1 and 3) with bleomycin at 12 µg/mL, or once (day 1) with mitomycin C at 1 µg/mL. After 5 days, micrographs were taken and cells were fixed with 3.7% formaldehyde and stained with crystal violet solution.

2.6. Western blot analysis

Cells were washed twice in cold PBS and lysed on ice with 2X Laemmli buffer (100 mM Tris pH 6.8, 20% glycerol, 4% SDS, 0.05% bromophenol blue and 10 mM DTT). Cell lysates were sonicated on ice and boiled at 96°C for 5 min. Twenty-five µg of proteins were resolved

on 12% or 15% SDS-PAGE and transferred to nitrocellulose membranes (Bio-Rad). Membranes were saturated with TBS supplemented with 0.05% Tween and 5% milk for 1 h at room temperature and incubated overnight at 4°C with primary antibodies against H-Ras (Santa Cruz Biotechnology, C-20); p53 (R&D Systems, AF1355); alpha-tubulin (Sigma, T6199). Primary antibodies were visualized with appropriate secondary antibodies conjugated to horseradish peroxidase: donkey anti-rabbit and sheep anti-mouse (Interchim), and donkey anti-goat (Santa Cruz Biotechnology) antibodies. Membrane development was performed using the ECL kit (Amersham), chemiluminescence detected and recorded using the Biorad Chemidoc system.

2.7. Microarray

After extraction, RNA quality (RIN index) was controlled using the 2200 TapeStation system (Agilent technology). Transcriptome analysis of MEFs was performed using Whole Mouse Genome Microarrays 4x44K v2 (Agilent Technologies) and the one-color gene expression Agilent workflow. Briefly, cRNAs were synthesized and labeled with Cy3 dye starting from 100 ng of total RNA extracted with the Nucleospin RNA kit (Macheray Nalgen), using the one-color Low Input Quick Amp Labeling Kit (Agilent Technologies). After labeling and quality control validation, 1650 ng of Cy3-labeled cRNAs were hybridized on the 4x44K arrays for 17 h at 65°C. Microarrays were washed and scanned with an Agilent DNA microarray scanner G2565CA (Agilent Technologies). Fluorescent signals were extracted using the Feature Extraction Software Version 10.5.1.1 (Agilent Technologies), and transferred to Genespring GX 12.6 software (Agilent Technologies) for data processing and data mining. Data were normalized in Genespring using the 75^{th} percentile method. Microarray probes were filtered using Agilent flag filter to remove probes with a raw signal below 20 in all the conditions tested. Differentially-expressed genes (DEGs) were defined

using moderated t-test p-value < 0.05 with a Benjamani-Hochberg correction and fold change cut-offs of 1.5-fold for up- and down-regulation. For Gene Ontology (GO) performed on DEG analysis we used the GO tool included into the Agilent Genespring software using default parameters. For data visualization, hierarchical clustering was performed with the Euclidian metric and complete linkage method.

2.8. Migration assay

Fifty thousand cells per well were seeded in 96-well plates (IncuCyte® ImagelockSartorius). The following day a scratch was performed using the IncuCyte® 96-Well Woundmaker Tool (Sartorius). After wounding, medium was discarded and cells were washed twice with 100 µL of warmed PBS before adding fresh medium. Images were acquired every hour by the IncuCyte™ system. Data were analysed by the wound confluence metric, one of the three integrated metrics calculated by custom algorithms that is part of the IncuCyte™ software package.

2.9. Sphere formation assay

Cells were washed, trypsinized, counted, and diluted to a concentration of 100,000 cells/mL in medium. Ten µL were deposited to the lid of a 10 cm in diameter culture dish as drops, the lid was carefully inverted and placed on the bottom of the plate filled with 10 mL PBS to avoid evaporation. The number of drops displaying spheres were after counted 5 days.

2.10. Animal care and in vivo procedures

C57Bl/6JRj mice (Janvier Labs) were maintained under standard conditions (standard diet and water *ad libitum*) at 23°C with 12 h light and 12 h dark cycles, in a specific pathogen-free (SPF) animal facility, P-PAC, at the Cancer Research Center of Lyon. Experiments were

conducted in accordance with the animal care guidelines of the European Union and French laws. Protocols were approved by the local Animal Ethics Evaluation Committee and authorized by the French Ministry of Education and Research (N° APAFIS#17226-2018092816251857V5).

For engraftment, transformed cells after senescence (TS) or non-senescent (T) cells were washed, trypsinized and prepared in 25% Matrigel (Corning® Matrigel® Matrix 2515249) in cold PBS at a concentration of 50 million cells/mL. One hundred µL were injected into the right flank of 7-week-old mice. The size of tumors was measured using a caliper.

2.11. Single cell RNA sequencing and analysis

Bioinformatics Analyses

All genomic data were analysed with R/Bioconductor packages, R version 4.1.1 (2021-08-10) [https://cran.r-project.org/, http://www.bioconductor.org/].

Single Cell RNA Sequencing

Poor quality and doublets were filtered out by retaining only cells with a library size ranging from 1,000 features to 10,000 features, and 5,000 cells of each condition (TS or T) were separated into nanoliter-scale Gel Bead-In-Emulsions (GEMs) with the Chromium Single Cell Controller (10X Genomics). After cell encapsulation and barcoding, library preparation followed the standard scRNAseq protocol comprising reverse transcription, amplification, and indexing (10xGenomics). Sequencing was performed using a NovaSeq Illumina device (Illumina). Illumina bcl files were basecalled, demultiplexed and aligned against the mouse mm10 genome using the cellranger software (version 3.1.0, 10X Genomics).

Raw counts were imported into R and single cell data were analysed with the ‘Seurat’ package v.3.2.2 [16]. After filtering for library size (between 1,000 and 10,000 features per cell) and mitochondrial gene expression (less than 10%), pre-processing was performed using

Seurat functions for count normalization (SCTransform regressing out in the percentage of mitochondrial genes), dimension reduction with principal component analysis (PCA) (RunPCA with default parameters), construction of a Shared Nearest Neighbor (SNN) graph (FindNeighbors using 10 dimensions of reduction as input) and clustering (FindClustering with a resolution of 0.2). Data were adjusted for cell cycle using the CellCycleScoring function and regressing for S and G2/M phase scores. After visualization with Uniform Manifold Approximation and Projection (UMAP) dimensional reduction technique [https://arxiv.org/abs/1802.03426], markers of each cluster were identified using the Wilcox test option of the FindAllMarkers function, with a Bonferroni p-value adjustment.

R packages 'pathfindR' version 1.6.2 [17] and 'enrichr' version 3.0 [18] were used to calculate pathway enrichment for each set of markers of clusters. Genelist scores at the single cell level were calculated with Seurat's AddModuleScore function, using 100 control features.

2.12. The Cancer Genome Atlas (TCGA) data

Harmonized TCGA data were accessed through The National Cancer Institute (NCI) Genomic Data Commons (GDC) using the 'TCGAbiolinks' package version 2.20.0 [19,20]. Count-level data were processed with the 'edgeR' package v.3.26.7 [https://doi.org/10.1093/bioinformatics/btp616]. Singscore (version 1.12.0) [21] was used to calculate scores for each sample based on selected gene lists. Tumor samples were then classified into two groups, Low and High, based on the median of different scores. Survival data (*i.e.* time to last follow-up and overall survival status) were used to fit a Cox proportional hazards regression model using the 'survival' package v.2.44-1.1 [https://CRAN.R-project.org/package=survival]. Survival Kaplan-Meier curves were plotted with 'survminer' v.0.4.5 [https://CRAN.R-project.org/package=survminer].

3. Results

3.1. Models of transformed cells arising from oncogenic stress-induced senescent cells or from proliferating cells

To investigate the impact of the sequence of transforming events, namely gain-of-oncogenes and loss-of-tumor suppressors, on tumor cell properties, we developed a cellular model based on MEFs which, compared to human cells, require a minimum number of genetic events to induce transformation [22-24]. MEFs were transduced with viral vectors encoding oncogenic RasV12 or a short hairpin RNA targeting mouse p53 mRNA (shp53) (Fig. 1A and Suppl. Fig.1A). As expected, the constitutive expression of RasV12 decreased cell density and promoted the SA-β-galatosidase compared to loss of p53 (shp53) (Fig. 1B and Suppl. Fig. 1B), indicating the induction of cellular senescence. Transcriptome analysis performed on MEFs transduced by RasV12 or shp53, also confirmed enrichment in cellular senescence-related signatures in RasV12-expressing cells, including down-regulation of genes involved in cell division, mitosis, and of apoptosis, and up-regulation of genes involved in inflammatory and oxidative responses, according to gene ontology analyses (GO) (Fig. 1C and Suppl. Fig. 1C-D). Importantly, the proliferation arrest induced by RasV12 was highly stable, as cells expressing RasV12 remained arrested (with no spontaneous escape) after 5 weeks of culture (Fig. 1D).

We then introduced RasV12 in proliferating shp53-expressing MEFs to generate transformed (T) cells or shp53 in RasV12-expressing senescent cells to allow these cells to resume proliferation and to generate transformed cells after senescence (TS) (Fig. 1A and 1E). After the second round of transduction, the two transformed MEF-derived cell lines harbored similar levels of RasV12 and p53, and could then be compared (Fig. 1E). In addition, T and TS cells displayed similar proliferation rates according to growth curve (Fig. 1F) and they reached confluency at the same time (Fig. 1G, upper panel).

Hence, we generated two models of cells possessing similar growth rates and bearing the same genetic alterations driving cellular transformation, but having previously undergone cellular senescence (TS cells) or not (T cells).

3.2. Transformed cells after senescence have a greater tumorigenic capacity and display more aggressive features than transformed non-senescent cells

Next, we compared tumor cell properties of transformed non-senescent cells (T) and transformed cells after senescence (TS) to define whether the sequence of genetic events leading to cell transformation impacted tumor cell properties. During crystal violet staining, we observed that TS cells grew more on top of each other than T cells (Figure 1G, lower panel, arrows), suggesting that an increased loss of contact inhibition, a mark of cell transformation [25], occurred in TS cells. We next assessed the ability of these cells to form spheroids under low-adherence conditions. Not only did TS cells form spheroids more readily than T cells (Fig. 2A), but they were also able to rapidly form tumors after subcutaneous engraftment in mice (Fig. 2B and Suppl. Fig. 2A).

Aside from this accelerated tumor growth rate, TS cells were more resistant to cell death induced by two anti-tumoral drugs, mitomycin C (Fig. 2C-D) and bleomycin (Suppl. Fig. 2B-C), and displayed an increased level of migration according to scratch assays (Fig. 2E-F).

Together, these results support that transformed cells generated from senescent cells display more aggressive tumor properties, including enhanced proliferation, resistance to cell death and an increased ability to migrate.

3.3. Transformed cells after senescence do not retain the transcriptomic profile of senescent cells but display a unique signature

To better understand the properties of transformed cells arising from senescent cells, we

performed bulk transcriptomic analyses of TS and T cells. First, we identified a large number of differentially-expressed genes (DEGs) between TS and T cells (Fig. 3A), indicating that the order of genetic events orchestrating the induction of cell transformation had a strong impact on gene expression profiles. We then analysed the senescence-associated signatures by gene ontology to verify whether signatures induced in MEFs by RasV12 (Fig. 1C), when compared to shp53-expressing cells, were conserved in TS cells, compared to T cells. Most of the signatures enriched in RasV12 senescent cells were not conserved in TS cells, except for the negative regulation of apoptosis (Fig. 3B).

Next, we investigated whether transformed cells arising from senescent cells displayed a greater cell heterogeneity, which could promote cell plasticity and could thus underlie the worse tumor phenotypes observed with TS cells [26]. To achieve this, we performed scRNA-seq experiments on TS and T cells, and observed that some of these cells clustered together and some did not, but mainly that the number of specific clusters was identical between the two, supporting that cell heterogeneity was similar (Fig. 3C-D and Suppl. Table 1). Nevertheless, some cell clusters were specific to the TS phenotype, providing us with the opportunity to identify a signature unique to cells having undergone senescence.

Collectively, these analyses rule out features such as SASP maintenance and increased cell heterogeneity as potential mechanisms underlying the pro-tumoral effects observed in TS cells, albeit they reveal some molecular marks specific to TS cells.

3.4. The transcriptomic signature of transformed cells after senescence is correlated with worse prognosis in human cancers

As TS cells display increased tumorigenesis, resistance and migration, all features associated with poor patient prognosis, we created a transcriptomic signature of TS cells and generated a molecular score, the prognostic value of which we assessed in cohorts of patients with cancer.

Based on bulk and single cell transcriptomic data, we initially selected DEGs common to TS vs T cells. Of these, 110 were down-regulated and 41 up-regulated in TS compared to T, and constituted our TS signature (Suppl. Table 2 and Fig. 4A). Using the singscore method [21], we then assessed the potential prognostic value of the molecular TS signature (or score) by querying The Cancer Genome Atlas (TCGA) (Table 1). Strikingly, a high TS score was correlated with a decreased survival probability in lung adenocarcinoma (LUAD) (Fig. 4B), head-neck squamous cell carcinoma (HSNC) (Fig. 4C), adrenocortical carcinoma (ACC) (Fig. 4D), liver hepatocellular carcinoma (LIHC) (Fig. 4E), skin cutaneous melanoma (SKCM) (Fig. 4F) and low-grade glioma (LGG) (Fig. 4G). None of the other tumor types displayed significant differences between a high and low TS score and their overall survival (Table 1).

Overall, these results demonstrate that a high TS score, derived from DEGs between transformed cells after senescence and transformed non-senescent cells, is correlated with worse survival in a subset of human cancers.

4. Discussion

In this study, we unveiled that cells entering senescence before undergoing transformation (TS) are more resistant to cell death induced by therapies, more motile and more tumorigenic in mice, compared to transformed non-senescent cells (T) having been subjected to the same oncogenic hits. Aside from the pro-tumoral phenotype of TS cells, we also identified a molecular signature specific to these cells by merging bulk and scRNA-seq transcriptomic data. Importantly, a higher score of this signature was correlated with decreased probability of survival for patients with different tumor types.

Transformation of normal cells requires gain-of-oncogenes and loss-of-tumor suppressor genes, though their order may vary in different tumor types and across different tumors of the same type. Here, we generated a simple model of transformed MEFs by varying the sequence of only two genetic events, namely the addition of RasV12 and removal of p53 to initiate transformation, whereas more are required for human cells [22-24]. We observed that cells arising from the sequential addition of RasV12 and loss-of-p53 are more aggressive as they display an increased ability to migrate, to resist cell death and to form tumors in mice. In line with these results, the transformation of normal bovine adrenocortical cells by first adding RasV12 and then a dominant negative form of p53 produced tumors with metastatic behaviors, whereas reversing the sequence of events gave rise only to benign tumors [27].

As expected, initiating the sequence with RasV12 expression [28] induced OIS, whereas this was not the case when expressed after p53 inhibition. Recent evidence supports that increased cellular senescence promotes tumor initiation and progression in several cellular or mouse models [7-14]. Albeit, according to our knowledge, we report for the first time that transforming cells after senescence leads to more aggressive behavior in the tumor cells generated.

Our attempt to better understand why transformed cells after senescence are more

dangerous than transformed non-senescent cells, did not reveal a clear mechanism but allowed us to propose hypotheses and to rule out others. Indeed, one hypothesis resides in the fact that after experiencing senescence, TS cells may conserve pro-tumoral properties of senescent cells. Such "senescent" properties could then confer advantages to TS cells such as cell death resistance [29] or increased SASP pro-inflammatory program [30]. Neither the SASP pro-inflammatory program is up-regulated in TS cells when compared to T cells. Interestingly, down-regulation of the gene signature associated with "regulation of apoptosis" in RasV12-induced senescent cells is conserved in TS cells vs T cells. We can thus speculate that this property contributes to the pro-tumoral properties of TS cells, as resistance to apoptosis participates in cell transformation and tumorigenicity [31] and promotes migration through the activation of non-lethal apoptosis regulators [32]. Another hypothesis to explain differences between TS cells and T cells may rely on the difference in cell heterogeneity, though scRNAseq analysis conducted herein does not support this hypothesis. Further work will be required to improve our understanding of the molecular properties induced by senescence and how this step subsequently confers pro-tumoral advantages to transformed cells. In particular, we focus here analysis on the transcriptomes but post-transcriptional alterations occurring in senescent cells, such as the translatome and protein turnover [33,34], could also contribute to TS cell properties.

Transcriptomic approaches were used herein to define the molecular signature, composed of up- and down-regulated genes, of TS cells compared to T cells. Whether some of these up- or down-regulated genes, alone or in combination, mediate TS cell behavior will need to be functionally tested in the future; this will be challenging as this signature contained 151 up- or down-regulated genes. Strikingly, examination of this signature across human tumor TCGA datasets, confirmed the more aggressive phenotype of TS cells as it was associated with worse patient survival in several cancers. Indeed, a high TS score was correlated with poor survival

for patients with lung adenocarcinoma, head-neck squamous cell carcinoma, adrenocortical carcinoma, liver hepatocellular carcinoma, skin cutaneous melanoma and low-grade glioma. Interestingly, the way these tumors develop might be associated with cellular senescence. For instance, melanocytic naevi are often associated with oncogene activation and cellular senescence, and their progression to melanoma can be linked with escape from senescence by loss-of-p53 and/or -p16 [35]. Whether a high TS score in a given tumor is an indicator of the history of the tumor and in particular whether this tumor underwent senescence prior to its transformation process remains unknown. New tumor models will be required to address this question.

5. Conclusion

A key finding of our study was the greater aggressive behavior of tumors arising from the transformation of senescent cells, as this is generally not considered when developing models of cancer cell behavior patterns (invasive properties, resistance to treatment…) either *in vitro* or *in vivo* in genetically-engineered mice. Indeed, generating transformed cells that did not undergo senescence will likely lead to less tumorigenic and aggressive tumors that will not reflect the complexity and behaviors of human tumors with the worse prognoses. Thus, using tumor models generated from senescent cells may be more relevant to understanding the etiology, progression as well as resistance to treatment of the most aggressive human tumors.

Abbreviations

ACC: adrenocortical carcinoma; DEG: differentially-expressed genes; EMT: epithelial-to-mesenchymal transition; FBS: fetal bovine serum; HSNC: head-neck squamous cell carcinoma; LGG: low-grade glioma; LIHC: liver hepatocellular carcinoma; LUAD: lung adenocarcinoma; MEF: mouse embryonic fibroblasts; OIS: oncogene-induced senescence; SASP: senescence-associated secretory program; SA-β-Galactosidase: senescence-associated-β-galactosidase; shRNA: short hairpin RNA; SKCM: skin cutaneous melanoma; T cells: transformed cells; TCGA: The Cancer Genome Atlas; TS cells: Transformed cells after senescence.

Declarations

Ethics approval and consent to participate

Experiments on mice were conducted in accordance with animal care guidelines of European Union and French laws. Protocols were approved by the local Animal Ethics Evaluation Committee and authorized by the French Ministry of Education and Research (N° APAFIS#17226-2018092816251857V5).

Consent for publication

Not applicable

Availability of data and material

All data generated or analysed during this study will be included as supplementary information upon acceptance. Transcriptomic data (bulk and single cell) will be deposited once the paper will be accepted for publication.

Competing interests

The authors declare no competing interest.

Acknowledgements

We thank the laboratory members, Nicolas Aznar and Gabriel Ichim for helpful discussions. We thank Brigitte Manship for critical reading of the manuscript. This work was carried out with the support of the Fondation ARC pour la recherche sur le cancer to DB, la Ligue régionale contre le cancer to JMF and by the Fondation pour la Recherche Médicale FRM to AP.

Author contributions

AP, HHV and JMF performed *in vitro* experiments. AP, DG, JJM and DV performed *in vivo* experiments. HHV and JMF performed bioinformatics analyses. AP, HHV, JMF and DB designed the experiments and the results were analysed by all the co-authors. JMF and DB designed the overall study and co-supervised the work. AP, HHV, JMF and DB wrote the

manuscript. All authors have read and agreed to the published version of the manuscript.

References

[1] D. Bernard, Instructive power of senescence, Nat. Rev. Mol. Cell Biol. 19 (2018) 618.

[2] Y. Sun, J.P. Coppe, E.W. Lam, Cellular Senescence: The Sought or the Unwanted? Trends Mol. Med. 24 (2018) 871-885.

[3] C.M. Beausejour, A. Krtolica, F. Galimi, M. Narita, S.W. Lowe, P. Yaswen, et al., Reversal of human cellular senescence: roles of the p53 and p16 pathways, Embo J 22 (2003) 4212-4222.

[4] M. Collado, J. Gil, A. Efeyan, C. Guerra, A.J. Schuhmacher, M. Barradas, et al., Tumour biology: Senescence in premalignant tumours, Nature 436 (2005) 642.

[5] M. Collado, M., Serrano, Senescence in tumours: evidence from mice and humans, Nat. Rev. Cancer 10 (2010) 51-57.

[6] T.W. Kang, T. Yevsa, N. Woller, L. Hoenicke, T. Wuestefeld, D. Dauch, et al., Senescence surveillance of pre-malignant hepatocytes limits liver cancer development, Nature 479 (2011) 547-551.

[7] F. Alimirah, T. Pulido, A. Valdovinos, S. Alptekin, E. Chang, E., Jones, et al., Cellular Senescence Promotes Skin Carcinogenesis through p38MAPK and p44/42MAPK Signaling. Cancer Res, 80 (2020) 3606-3619.

[8] N. Azazmeh, B. Assouline, E. Winter, S. Ruppo, Y. Nevo, A. Maly, et al., Chronic expression of p16(INK4a) in the epidermis induces Wnt-mediated hyperplasia and promotes tumor initiation, Nat. Commun. 11 (2020) 2711.

[9] J.P. Coppe, C.K., Patil, F., Rodier, Y. Sun, D..P. Munoz, J. Goldstein, et al., Senescence-associated secretory phenotypes reveal cell-nonautonomous functions of

oncogenic RAS and the p53 tumor suppressor, PLoS Biol 6 (2008) 2853-2868.

[10] J.P. Coppe, P.Y. Desprez, A. Krtolica, J. Campisi, The senescence-associated secretory phenotype: the dark side of tumor suppression, Annu. Rev. Pathol. 5 (2010) 99-118.

[11] T. Eggert, K. Wolter, J. Ji, C. Ma, T. Yevsa, S. Klotz, et al., Distinct Functions of Senescence-Associated Immune Responses in Liver Tumor Surveillance and Tumor Progression, Cancer Cell 30 (2006)533-547.

[12] M. Milanovic, D.N.Y. Fan, D. Belenki, J.H.M. Dabritz, Z. Zhao, Y. Yu, et al., Senescence-associated reprogramming promotes cancer stemness, Nature 553 (2018) 96-100.

[13] L. Mosteiro, C. Pantoja, N. Alcazar, R.M. Marion, D. Chondronasiou, M. Rovira, et al., Tissue damage and senescence provide critical signals for cellular reprogramming in vivo, Science 2016, 354.

[14] J. Nassour, S. Martien, N. Martin, E. Deruy, E. Tomellini, N. Malaquin, et al., Defective DNA single-strand break repair is responsible for senescence and neoplastic escape of epithelial cells, Nat. Commun. 7 (2016) 10399.

[15] F. Debacq-Chainiaux, J.D. Erusalimsky, J. Campisi, O. Toussaint, Protocols to detect senescence-associated beta-galactosidase (SA-betagal) activity, a biomarker of senescent cells in culture and in vivo, Nat. Protoc. 4 (2009) 1798-1806.

[16] T. Stuart, A. Butler, P. Hoffman, C. Hafemeister, E. Papalexi, V.M.III.. Mauck, et al., Comprehensive Integration of Single-Cell Data, Cell 177 (2019) 1888-1902.

[17] E. Ulgen, O. Ozisik, O.U. Sezerman, pathfindR: An R Package for Comprehensive Identification of Enriched Pathways in Omics Data Through Active Subnetworks, Front

Genet. 10 (2019) 858.

[18] M.V. Kuleshov, M.R. Jones, A.D. Rouillard, N.F. Fernandez, Q. Duan, Z. Wang, et al., Enrichr: a comprehensive gene set enrichment analysis web server 2016 update, Nucleic Acids Res. 44 (2016) W90-W97.

[19] A. Colaprico, T.C. Silva, C. Olsen, L. Garofano, C. Cava, D. Garolini, et al., TCGAbiolinks: an R/Bioconductor package for integrative analysis of TCGA data, Nucleic Acids Res. 44 (2016) e71.

[20] T.C. Silva, A. Colaprico, C. Olsen, F. D'Angelo, G. Bontempi, M. Ceccarelli, M., et al., TCGA Workflow: Analyze cancer genomics and epigenomics data using Bioconductor packages, F1000Res. 5 (2016) 1542.

[21] M. Foroutan, D.D. Bhuva, R. Lyu, K. Horan, J. Cursons, M.J. Davis, Single sample scoring of molecular phenotypes, BMC. Bioinformatics. 19 (2018) 404.

[22] W.C. Hahn, R.A. Weinberg, Rules for making human tumor cells, N. Engl. J. Med. 347 (2002) 1593-1603.

[23] H. Land, L.F. Parada, R.A. Weinberg, Tumorigenic conversion of primary embryo fibroblasts requires at least two cooperating oncogenes, Nature 304 (1983) 596-602.

[24] R.A. Weinberg, Oncogenes, antioncogenes, and the molecular bases of multistep carcinogenesis, Cancer Res. 49 (1989) 3713-3721.

[25] D. Hanahan, R.A. Weinberg, Hallmarks of cancer: the next generation, Cell 144 (2011) 646-674.

[26] F. Luond, S. Tiede, G. Christofori, Breast cancer as an example of tumour heterogeneity

and tumour cell plasticity during malignant progression, Br. J. Cancer 125 (2021) 164-175.

[26] M. Herbet, A. Salomon, J.J. Feige, M. Thomas, Acquisition order of Ras and p53 gene alterations defines distinct adrenocortical tumor phenotypes, PLoS. Genet. 8 (2012) e1002700.

[27] M. Serrano, A.W. Lin, M.E. McCurrach, D. Beach, S.W. Lowe, Oncogenic ras provokes premature cell senescence associated with accumulation of p53 and p16INK4a, Cell 88 (1997) 593-602.

[29] L. Hu, H. Li, M. Zi, W. Li, J. Liu, Y. Yang, et al., Why Senescent Cells Are Resistant to Apoptosis: An Insight for Senolytic Development, Front Cell Dev. Biol. 10 (2022) 822816.

[30] M. Takasugi, Y. Yoshida, E. Hara, N. Ohtani, The role of cellular senescence and SASP in tumour microenvironment, FEBS J. 2022.

[31] P.A. Amstad, H. Liu, M. Ichimiya, S. Chang, I.K. Berezesky, B.F. Trump, bcl-2 enhancement of malignant transformation in mouse epidermal JB6 cells, Mol. Carcinog. 20 (1997) 231-239.

[32] K. Berthenet, F.C. Castillo, D. Fanfone, N. Popgeorgiev, D. Neves, P. Bertolino, et al., Failed Apoptosis Enhances Melanoma Cancer Cell Aggressiveness, Cell Rep. 31 (2020) 107731.

[33] X. Deschenes-Simard, M.F. Gaumont-Leclerc, V. Bourdeau, F. Lessard, O, Moiseeva, V. Forest, et al., Tumor suppressor activity of the ERK/MAPK pathway by promoting selective protein degradation, Genes Dev. 27 (2013) 900-915.

[34] M.J. Payea, C. Anerillas, R. Tharakan, M. Gorospe, Translational Control during Cellular Senescence, Mol. Cell Biol. 41 (2021) e00512-20.

[35] C. Michaloglou, L.C. Vredeveld, M.S. Soengas, C. Denoyelle, T. Kuilman, C.M. van der Horst, et al., BRAFE600-associated senescence-like cell cycle arrest of human naevi, Nature 436 (2005) 720-724.

Figure Legends

Fig. 1. Generation of transformed cells arising from proliferating or senescent cells. (A) Schematic representation of the experimental design allowing the generation of transformed MEFs arising either from proliferating cells (bottom), named transformed cells (T), or from senescent cells (top), named transformed MEFs after senescence (TS). RasV12 and shp53 indicate the two genetic modifications applied for MEF transformation. Six days after the first round of infection cells were seeded for the different assays to characterize cells including the senescence state (B-D), or for a second round of infection (E-G). **(B-D)** MEFs were infected with retroviral vector encoding RasV12 (RasV12) or lentiviral vector encoding shRNA targeting Trp53 (shp53). One week after infection cells were seeded at the same density. **(B)** Five days later they were fixed and crystal violet stained. **(C)** Two days later, RNAs were prepared and their transcriptomes analysed by microarrays. Gene Ontology (GO) analyses were performed, and some GO on differentially-expressed genes are shown. **(D)** Microscopic images of RasV12 or shp53 MEFs after 5 weeks of culture without cell splitting, (scale bar = 100 µm). **(E-G)** shp53-expressing cells were infected with RasV12 encoding vector to generate T cells and RasV12-expressing cells were infected with shp53 encoding vector to generate TS cells and the cells were puromycin selected and amplified during 2-3 weeks before performing the different assays. **(E)** Western blot analysis of p53 and Ras proteins in TS and T cells. Non-infected MEFs were used as control (ctrl). Nutlin was added to stabilize p53. Tubulin expression is used as a loading control. **(F)** Growth curve assays were performed on TS and T cells. **(G)** Crystal violet staining was performed on TS and T cells to visualize cell density 5 days after seeding (upper panel). Zoomed images are also shown (scale bar 50 µM) (lower panel).

Fig. 2. Transformed cells after senescence (TS) harbor worse tumor phenotypes than

transformed (T) non-senescent cells. (**A**) One thousand TS and T cells per droplet were seeded in low adherence conditions and analysed 5 days later. Left panel, microscopic images of spheres from TS and T cells. Right panel, quantification of the percentage of droplets displaying spheres (n = 4, mean +/- SEM, two-tailed unpaired t test **** $p < 0.0001$). (**B**) Five million TS and T cells were subcutaneously engrafted in mice. Tumor size was measured 11 days later. (n = 6 per group, mean, two-tailed unpaired t test, ** $p < 0.01$). **(C-D)** The day after seeding, TS and T cells were treated or not with 1 µg/mL Mitomycin C. Five days later, images were acquired (scale bar = 100 µm) and index of survival calculated **(C)**, and cells were fixed and crystal violet stained **(D)**. **(E-F)** TS and T cells were seeded in 96-well plates, and the day after scratches were performed. Images were acquired automatically using the IncuCyte system. **(E)** Images are shown at T0 immediately after the scratch and 15 h later. **(F)** Quantification of wounding over time in hours after scratch for TS or T cells (n = 4 per group, mean+/-SEM, paired t test, **** $p < 0.0001$).

Fig. 3. Transcriptomic analysis of transformed cells after senescence (TS) and transformed (T) non-senescent cells using microarray and scRNAseq. (A-B) RNAs of TS and T cells were prepared and transcriptomes analysed by microarrays. **(A)** Differentially-expressed genes (DEGs) are shown on a Volcano plot. Significant DEGs with fold change > 1.5 and q-value < 0.05 are shown in blue for down-regulated genes (down) and red for up-regulated ones (up). **(B)** Gene Ontology (GO) analysis of the transcriptomic data using Genespring software Gene Ontology tool. X axis represents the –log10(q-value). **(C-D)** scRNA-seq on TS and T cells. **(C)** tSNE plot visualization of clusters identified by scRNAseq by mixing TS and T cells and heatmap of the top 5 key markers of each cluster are shown. **(D)** tSNE plot representation similar to C with labelling of the identity of T cells in orange and TS cells in blue.

Fig. 4. The molecular signature of transformed cells after senescence (TS) is correlated with poor patient prognosis. (A) Venn diagram analysis identifying common differentially expressed genes between TS and T cells using bulk transcriptomes and TS-specific clusters according to scRNA-seq data. (**B-G)** Kaplan-Meier analyses of overall survival showing significant differences between high and low TS scores. TS signature scores were calculated using the singscore method across transcriptomic data of tumors from the TCGA database. High and low TS tumors were separated using the median for each tumor type and overall survival was analysed by Kaplan Meier plot for each tumor type. Only tumor types showing a significant prognostic value of the TS score are shown. HNSC (Head and Neck Squamous Cell Carcinomas); LUAD (Lung Adenocarcinoma); ACC (Adrenocortical carcinoma); LIHC (Liver Hepatocellular Carcinoma); LGG (Low Grade Glioma); SKCM (Skin cutaneous melanoma).

Figure 1

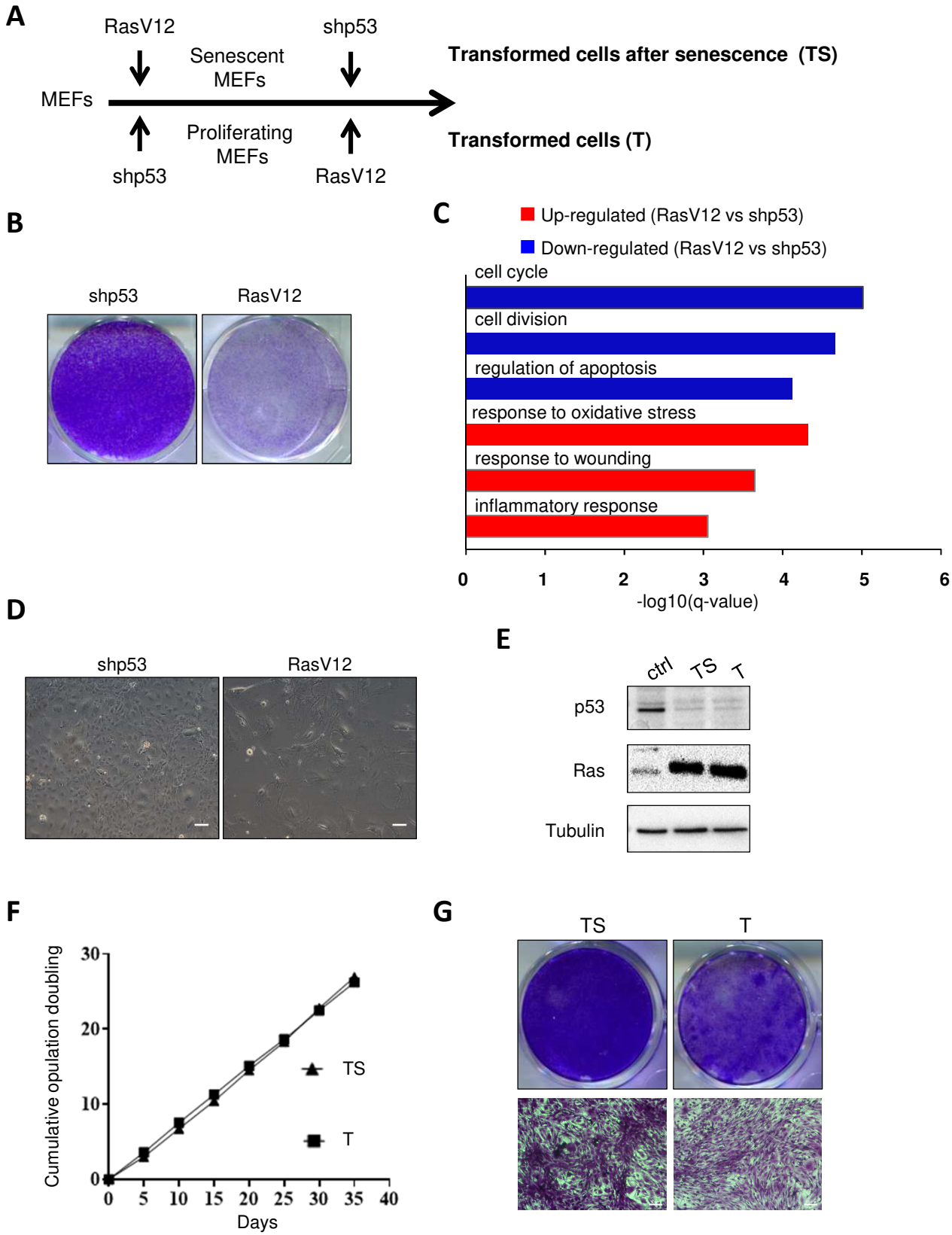
A
RasV12
shp53
Senescent MEFs
MEFs
Transformed cells after senescence (TS)
Proliferating MEFs
Transformed cells (T)
shp53
RasV12
B
shp53
RasV12
C
Up-regulated (RasV12 vs shp53)
Down-regulated (RasV12 vs shp53)
cell cycle
cell division
regulation of apoptosis
response to oxidative stress
response to wounding
inflammatory response
0
1
2
3
4
5
6
-log10(q-value)
D
shp53
RasV12
E
ctrl
TS
T
p53
Ras
Tubulin
F
Cumulative opulation doubling
30
20
10
0
0
5
10
15
20
25
30
35
40
Days
TS
T
G
TS
T

Figure 2

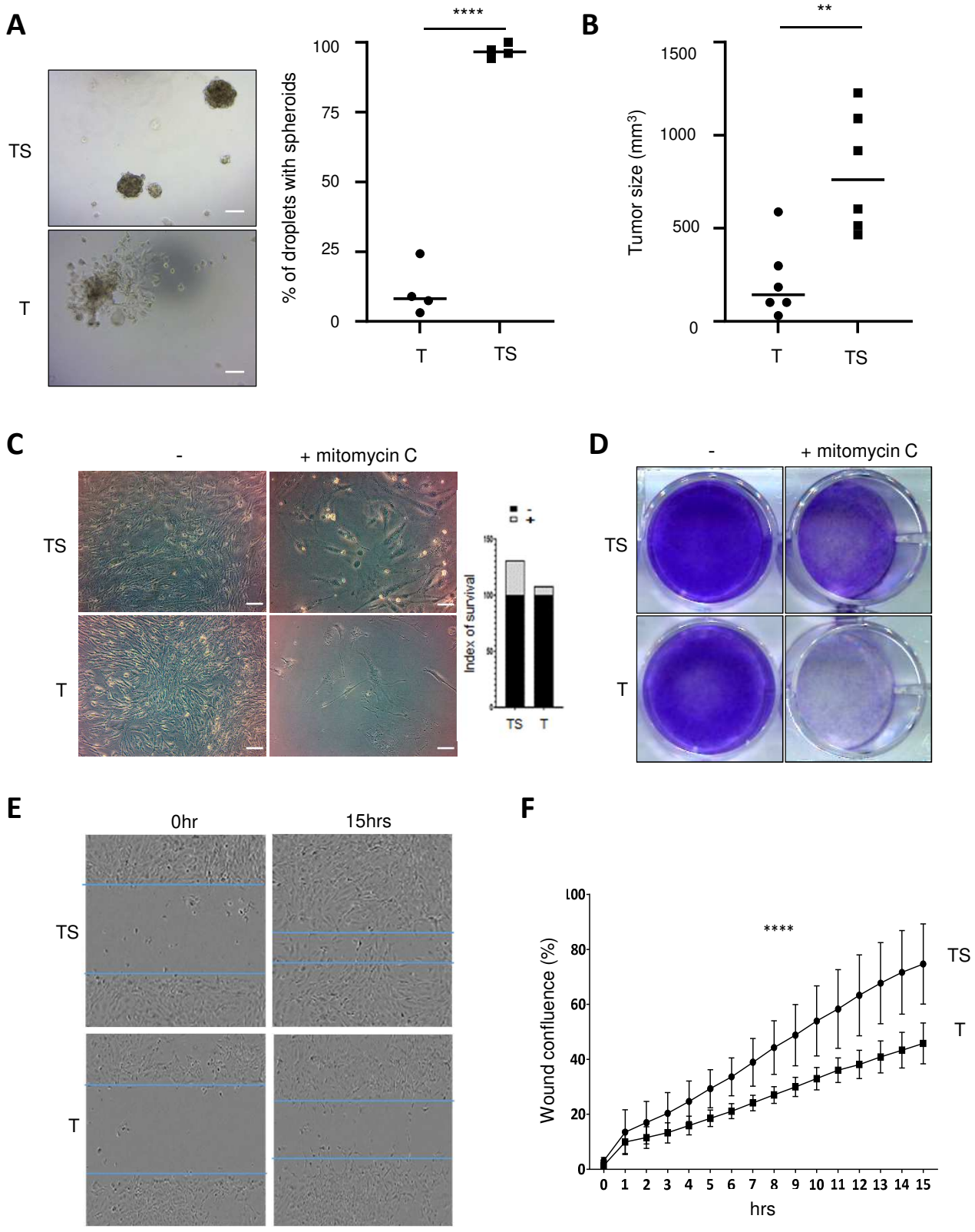
A
TS
T
****
100
75
50
25
0
% of droplets with spheroids
T
TS
B
**
1500
1000
500
0
Tumor size (mm3)
T
TS
C
-
+ mitomycin C
TS
T
Index of survival
TS
T
D
-
+ mitomycin C
TS
T
E
0hr
15hrs
TS
T
F
****
100
80
60
40
20
0
Wound confluence (%)
0 1 2 3 4 5 6 7 8 9 10 11 12 13 14 15
hrs
TS
T

Figure 3

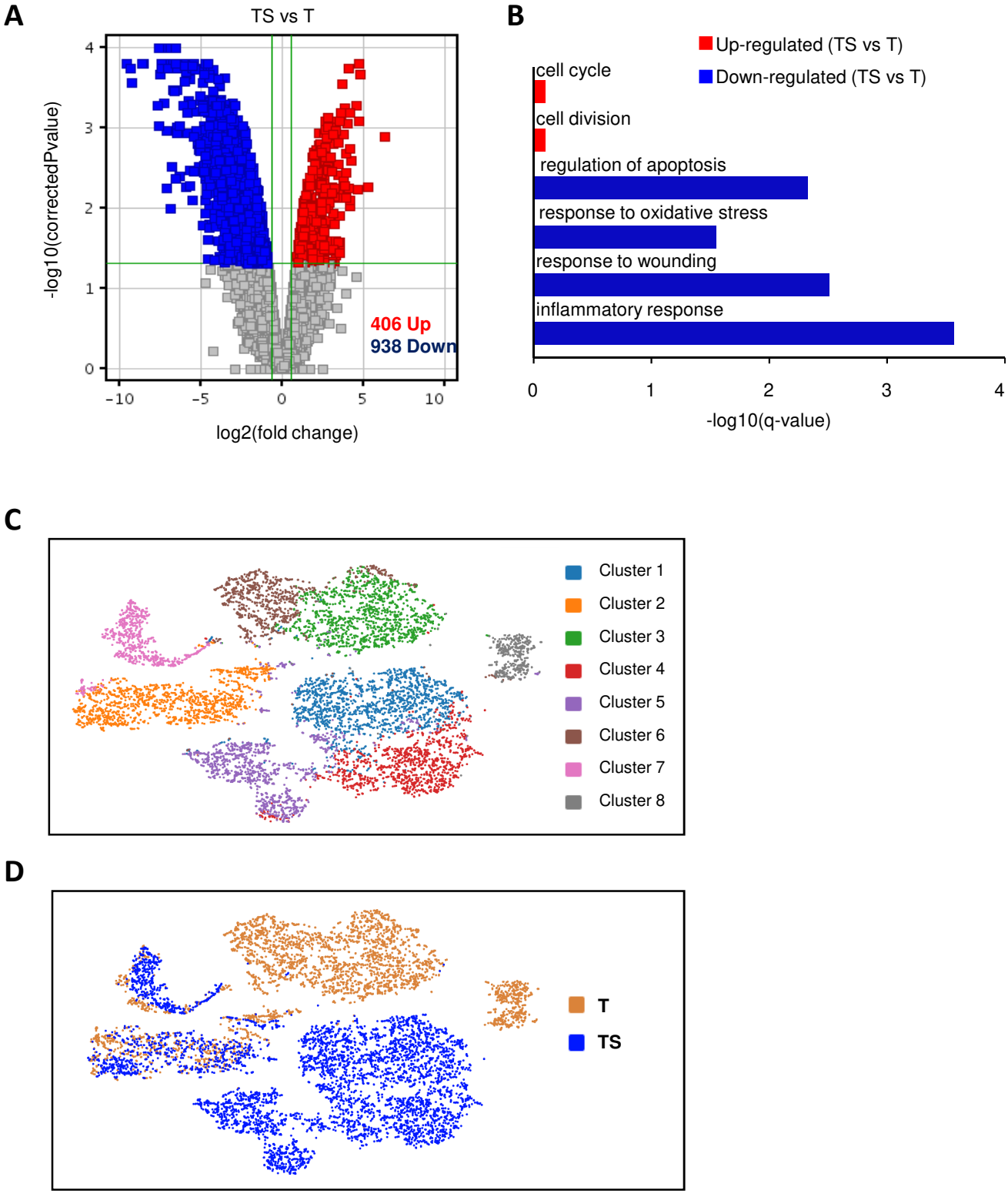
A
TS vs T
-log10(correctedPvalue)
log2(fold change)
406 Up
938 Down
B
Up-regulated (TS vs T)
Down-regulated (TS vs T)
cell cycle
cell division
regulation of apoptosis
response to oxidative stress
response to wounding
inflammatory response
-log10(q-value)
C
Cluster 1
Cluster 2
Cluster 3
Cluster 4
Cluster 5
Cluster 6
Cluster 7
Cluster 8
D
T
TS

Figure 4

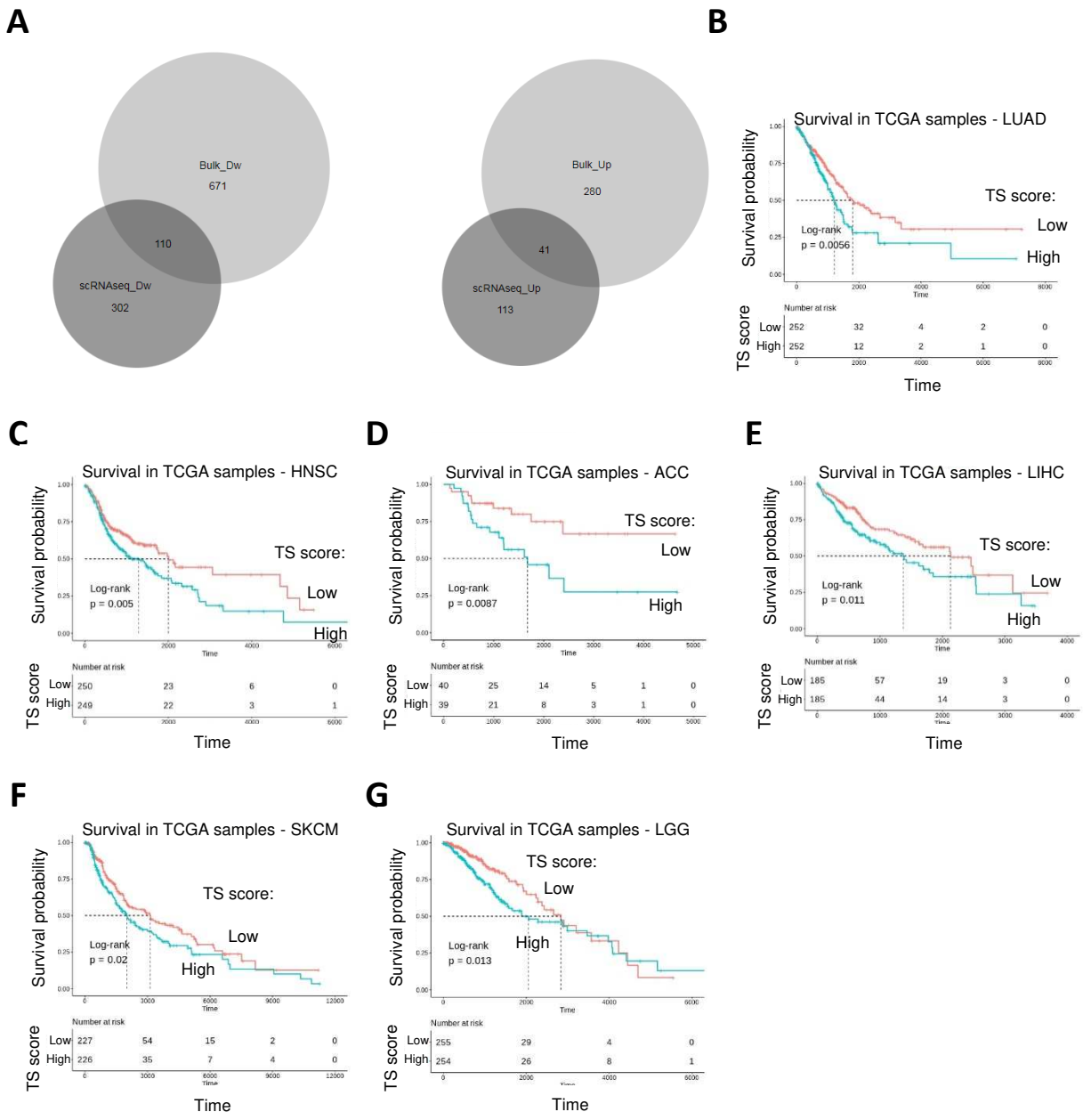
A
Bulk_Dw
671
110
scRNAseq_Dw
302
Bulk_Up
280
41
scRNAseq_Up
113
B
Survival in TCGA samples - LUAD
Survival probability
TS score:
Low
High
Log-rank
p = 0.0056
Number at risk
TS score
Low 252 32 4 2 0
High 252 12 2 1 0
Time
C
Survival in TCGA samples - HNSC
Survival probability
TS score:
Low
High
Log-rank
p = 0.005
Number at risk
TS score
Low 250 23 6 0
High 249 22 3 1
Time
D
Survival in TCGA samples - ACC
Survival probability
TS score:
Low
High
Log-rank
p = 0.0087
Number at risk
TS score
Low 40 25 14 5 1 0
High 39 21 8 3 1 0
Time
E
Survival in TCGA samples - LIHC
Survival probability
TS score:
Low
High
Log-rank
p = 0.011
Number at risk
TS score
Low 185 57 19 3 0
High 185 44 14 3 0
Time
F
Survival in TCGA samples - SKCM
Survival probability
TS score:
Low
High
Log-rank
p = 0.02
Number at risk
TS score
Low 227 54 15 2 0
High 226 35 7 4 0
Time
G
Survival in TCGA samples - LGG
Survival probability
TS score:
Low
High
Log-rank
p = 0.013
Number at risk
TS score
Low 255 29 4 0
High 254 26 8 1
Time

Tumors	beta	HR (95% CI for HR)	wald,test	p,value
HNSC	**0.38**	**1.5 (1.1-1.9)**	**7.8**	**0.005**
LUAD	**0.41**	**1.5 (1.1-2)**	**7.6**	**0.0056**
ACC	**1**	**2.8 (1.3-6.2)**	**6.3**	**0.0087**
LIHC	**0.45**	**1.6 (1.1-2.2)**	**6.3**	**0.011**
LGG	**0.46**	**1.6 (1.1-2.3)**	**6**	**0.013**
SKCM	**0.32**	**1.4 (1.1-1.8)**	**5.4**	**0.02**
STAD	-0.32	0.72 (0.52-1)	3.8	0.052
OV	0.25	1.3 (0.98-1.7)	3.4	0.066
KICH	1.3	3.6 (0.75-17)	2.6	0.087
KIRP	-0.45	0.64 (0.35-1.2)	2.1	0.14
KIRC	0.17	1.2 (0.88-1.6)	1.3	0.26
PRAD	0.76	2.1 (0.55-8.3)	1.2	0.26
CHOL	0.45	1.6 (0.61-4)	0.87	0.35
UVM	0.4	1.5 (0.64-3.5)	0.85	0.35
TGCT	-1	0.35 (0.037-3.4)	0.81	0.35
SARC	0.18	1.2 (0.8-1.8)	0.78	0.38
BLCA	0.11	1.1 (0.83-1.5)	0.58	0.45
LUSC	-0.1	0.9 (0.69-1.2)	0.54	0.46
ESCA	0.18	1.2 (0.73-2)	0.53	0.47
MESO	0.17	1.2 (0.74-1.9)	0.51	0.47
READ	0.29	1.3 (0.6-2.9)	0.51	0.47
THCA	0.35	1.4 (0.53-3.8)	0.49	0.48
PAAD	0.13	1.1 (0.75-1.7)	0.37	0.54
UCEC	0.12	1.1 (0.74-1.7)	0.31	0.58
COAD	0.087	1.1 (0.74-1.6)	0.19	0.66
BRCA	0.07	1.1 (0.78-1.5)	0.19	0.67
GBM	0.078	1.1 (0.76-1.5)	0.18	0.67
CESC	-0.099	0.91 (0.57-1.4)	0.17	0.68
UCS	0.14	1.1 (0.58-2.3)	0.16	0.69
PCPG	-0.058	0.94 (0.19-4.7)	0.01	0.94
DLBC	-0.025	0.98 (0.24-3.9)	0	0.97
THYM	0.029	1 (0.26-4)	0	0.97

Table 1: List of overall survival Kaplan Meier plots performed using the transformed senescent (TS) signature score across TCGA database. The TS score was calculated using the singscore method and samples with TS high versus TS low scores were split at the median. Tumors for which the TS signature with a high score has a significant prognostic value are indicated in bold.

Supplemental Table 1

	FeatureID	FeatureName	Log2 Fold Change	P-Value
cluster 1	ENSMUSG00000000031	H19	-6.80627133588865	1.43E-239
	ENSMUSG00000039114	Nrn1	-6.1178975367657	6.49E-200
	ENSMUSG00000028037	Ifi44	-5.99587550948102	3.59E-199
	ENSMUSG00000054072	Iigp1	-6.36835510658066	1.85E-197
	ENSMUSG00000094777	Hist1h2ap	-5.91069292604075	1.07E-196
	ENSMUSG00000030921	Trim30a	-6.09085446519757	3.25E-191
	ENSMUSG00000024529	Lox	-5.6866911406378	1.10E-178
	ENSMUSG00000069171	Nr2f1	-5.08416875969674	2.82E-164
	ENSMUSG00000030218	Mgp	-5.08432247451787	2.58E-159
	ENSMUSG00000024087	Cyp1b1	-7.4633549348586	2.24E-158
cluster 2	ENSMUSG00000027022	Xirp2	10.2512470041314	4.81E-10
	ENSMUSG00000105361	AY036118	2.35185060484833	3.48E-05
	ENSMUSG00000042622	Maff	1.63069092820878	0.009157168
	ENSMUSG00000003545	Fosb	-2.64730459997596	0.009906835
	ENSMUSG00000094777	Hist1h2ap	-2.80530416173481	0.009906835
	ENSMUSG00000021250	Fos	-2.69084912135664	0.009906835
	ENSMUSG00000027200	Sema6d	-2.23633812063041	0.11160955
	ENSMUSG00000035202	Lars2	1.48006299906505	0.11160955
	ENSMUSG00000024087	Cyp1b1	-2.47846256307634	0.11160955
	ENSMUSG00000038418	Egr1	-2.09201171833643	0.11160955
cluster 3	ENSMUSG00000001657	Hoxc8	-4.9189675787103	3.20E-228
	ENSMUSG00000001661	Hoxc6	-4.7275533419991	2.22E-208
	ENSMUSG00000094777	Hist1h2ap	3.01913357227478	3.91E-194
	ENSMUSG00000048078	Tenm4	-4.81885999244965	7.70E-190
	ENSMUSG00000097910	5033428I22Rik	-4.89872757974825	3.15E-185
	ENSMUSG00000022037	Clu	-3.8881424319801	7.65E-177
	ENSMUSG00000036139	Hoxc9	-4.06975003973963	1.72E-162
	ENSMUSG00000021087	Rtn1	-5.28442274181033	9.30E-155
	ENSMUSG00000037362	Nov	-4.36670427363876	3.35E-154
	ENSMUSG00000028871	Rspo1	-5.54499109331543	7.09E-146
cluster 4	ENSMUSG00000030218	Mgp	-7.66309623372425	5.82E-221
	ENSMUSG00000039114	Nrn1	-7.32543639574493	3.57E-208
	ENSMUSG00000054072	Iigp1	-7.66612408883383	5.12E-204
	ENSMUSG00000028037	Ifi44	-6.8184560908103	1.94E-202
	ENSMUSG00000030921	Trim30a	-6.92741816622172	4.21E-192
	ENSMUSG00000000031	H19	-5.59961508567511	7.85E-186
	ENSMUSG00000079017	Ifi27l2a	-5.64556786261083	1.77E-162
	ENSMUSG00000029561	Oasl2	-5.22723716975683	2.71E-162
	ENSMUSG00000024529	Lox	-5.36144896879105	2.02E-157
	ENSMUSG00000024087	Cyp1b1	-9.14081076613865	3.20E-154
cluster 5	ENSMUSG00000028871	Rspo1	4.31742071500197	4.22E-297
	ENSMUSG00000048251	Bcl11b	3.41063137231648	1.65E-168
	ENSMUSG00000096225	Lhx8	3.13039991179544	4.00E-160
	ENSMUSG00000000031	H19	-5.40816530086177	4.20E-135
	ENSMUSG00000030921	Trim30a	-6.18425031236066	1.79E-134
	ENSMUSG00000054072	Iigp1	-5.85046257271722	2.11E-129
	ENSMUSG00000079017	Ifi27l2a	-5.96494754428252	2.62E-128
	ENSMUSG00000045475	Lce3c	4.56496759894093	3.67E-127
	ENSMUSG00000030218	Mgp	-5.37832767298062	4.96E-120
	ENSMUSG00000024529	Lox	-5.37821361568685	5.10E-119
cluster 6	ENSMUSG00000030218	Mgp	4.49252442439973	1.47E-263
	ENSMUSG00000027750	Postn	5.36442473657142	4.77E-248
	ENSMUSG00000037206	Islr	4.74791683234914	8.35E-240
	ENSMUSG00000090942	F830016B08Rik	4.32566716807248	1.86E-228
	ENSMUSG00000022548	Apod	5.070747417666	7.85E-221
	ENSMUSG00000073555	Gm4951	4.08111485825804	1.74E-217
	ENSMUSG00000079017	Ifi27l2a	3.97500807634798	3.94E-214
	ENSMUSG00000000402	Egfl6	5.14224653014044	2.07E-205
	ENSMUSG00000054072	Iigp1	3.71698990929202	7.99E-195
	ENSMUSG00000021388	Aspn	3.87705559866524	5.57E-190
cluster 7	ENSMUSG00000064356	mt-Atp8	4.99189487892984	3.44E-39
	ENSMUSG00000064357	mt-Atp6	4.62505239807394	2.08E-35
	ENSMUSG00000064368	mt-Nd6	5.09797554188619	2.08E-35
	ENSMUSG00000064360	mt-Nd3	4.5313237063721	7.57E-33
	ENSMUSG00000064358	mt-Co3	4.49758247316398	2.55E-32
	ENSMUSG00000064354	mt-Co2	4.47337324776158	7.98E-32
	ENSMUSG00000064345	mt-Nd2	4.42246545394678	1.46E-30
	ENSMUSG00000064370	mt-Cytb	4.3714333480822	1.99E-29
	ENSMUSG00000065947	mt-Nd4l	4.41622679750495	7.45E-29
	ENSMUSG00000064363	mt-Nd4	4.21088758839427	5.62E-26
cluster 8	ENSMUSG00000000938	Hoxa10	6.25303437865147	0
	ENSMUSG00000045573	Penk	5.32542732943328	2.23E-239
	ENSMUSG00000056888	Glipr1	5.4091652585749	1.53E-179
	ENSMUSG00000038227	Hoxa9	4.21658768619089	2.15E-166
	ENSMUSG00000038210	Hoxa11	6.97366365673634	2.57E-159
	ENSMUSG00000020911	Krt19	4.29970786009593	5.11E-145
	ENSMUSG00000051022	Hs3st1	4.20664543269739	2.76E-139
	ENSMUSG00000015619	Gata3	3.82894594907941	2.42E-137
	ENSMUSG00000046733	Gprc5a	3.93210340267846	4.05E-130
	ENSMUSG00000035566	Pcdh17	3.41529645453418	1.89E-126

Suppl. Table 1 List of the top 10 genes defining the clusters.

Supplemental Table 2

Down-regulated genes	Up-regulated genes
Adam23; Atp1b1; Bgn; C1qtnf4; Casp12; Cbr3; Ccdc80; Cdh6; Cdk14; Cdo1; Cebpd; Ch25h; Chst15; Cmpk2; Crip2; Crlf1; Cxxc5; Cyp1b1; Cyth3; Dusp1; Ebf2; Ebf3; Eng; Ets2; F830016B08Rik; Fads3; Fam213b; Fgf2; Fgf7; Fmr1; Foxp1; Fxyd5; Gata3; Gbp2; Gm4951; Gpm6b; Gpx3; Gria3; H19; Heph; Hoxa10; Hoxa2; Hoxa3; Hoxa5; Hs3st1; Hs6st2; Ifi203; Ifi44; Ifi47; Ifit3; Igfbp7; Iigp1; Irgm2; Jam2; Kctd12b; Lox; Lpl; Ltbp2; Ltbr; Map2; Mdk; Mgp; Mndal; Mtcl1; Ndn; Nr2f1; Nrgn; Nrn1; Nrp1; Nsg1; Oasl2; Pde8b; Pdgfa; Peg3; Penk; Phf11d; Plscr2; Plxdc2; Plxna2; Pmp22; Ptgis; Ptgs2; Rbp1; Rnf213; Serpine2; Sfrp1; Sgk1; Shox2; Six2; Slc14a1; Slfn8; Slit2; Snai1; Sned1; Socs5; Sp100; Spp1; Tbx1; Tbx2; Tcfl5; Tmem176b; Trib2; Trim12a; Trim12c; Trim30a; Trim30d; Trim34a; Tspan4; Tspan6; Xaf1	5033428I22Rik; Adcy8; Anxa5; Apobr; Atp6v0e2; Cnr1; Cpe; Crip1; Ctsk; Dkk2; Ebf1; Eml5; Fjx1; Gpr149; Hand2; Hoxb5; Hoxb9; Hoxc6; Hoxc8; Hoxc9; Irx2; Irx3; Itga2; Jade1; Lbh; Lin7a; Notch2; Npepl1; Plekhb2; Ptprd; Pxdc1; Rtn1; Sema3a; Sfmbt2; Sh2d5; Six1; Six4; Sprr1a; Syne1; Tenm4; Tpd52

Suppl. Table 2 List of genes used to define the TS score.

Supplemental Figure 1

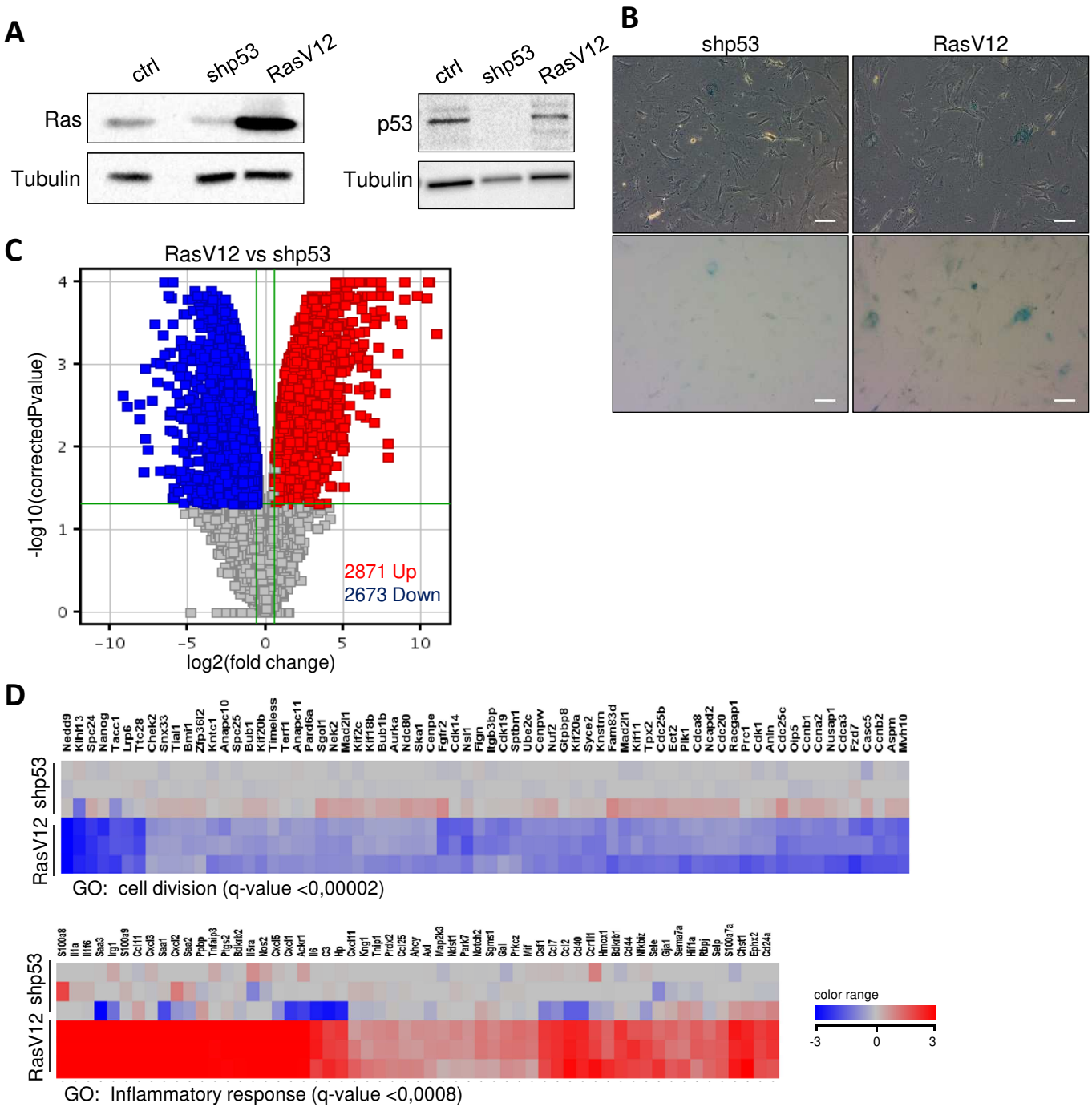

Suppl. Fig. 1 RasV12 expression in MEFs induces senescence. MEFs were infected with shp53- or RasV2-expressing vectors and selected. Two days later the different assays were performed. **(A)** Cell lysates were prepared and Western blot analysis against p53 and Ras performed 2 days after seeding. Non-infected MEFs were used as a control (ctrl) and tubulin expression was used as a loading control. **(B)** SA-β-galactosidase assays were performed 2 days after seeding. Representative micrographs are shown (scale bar= 50 µm). **(C)** Volcano plot representation of transcriptomic data from RasV12-encoding MEFs vs shp53-expressing MEFs. Differentially-expressed genes (DEGs) in RasV12 condition with Fold Change >1.5 and q-value <0.05 are shown in blue for down-regulated genes and in red for up-regulated ones. **(D)** Heatmap representation of DEGs between RasV12- vs shp53-encoding MEFs which are significantly enriched in Gene Ontology (GO) cell division or inflammatory response according to Agilent Genespring software GO tool.

Supplemental Figure 2

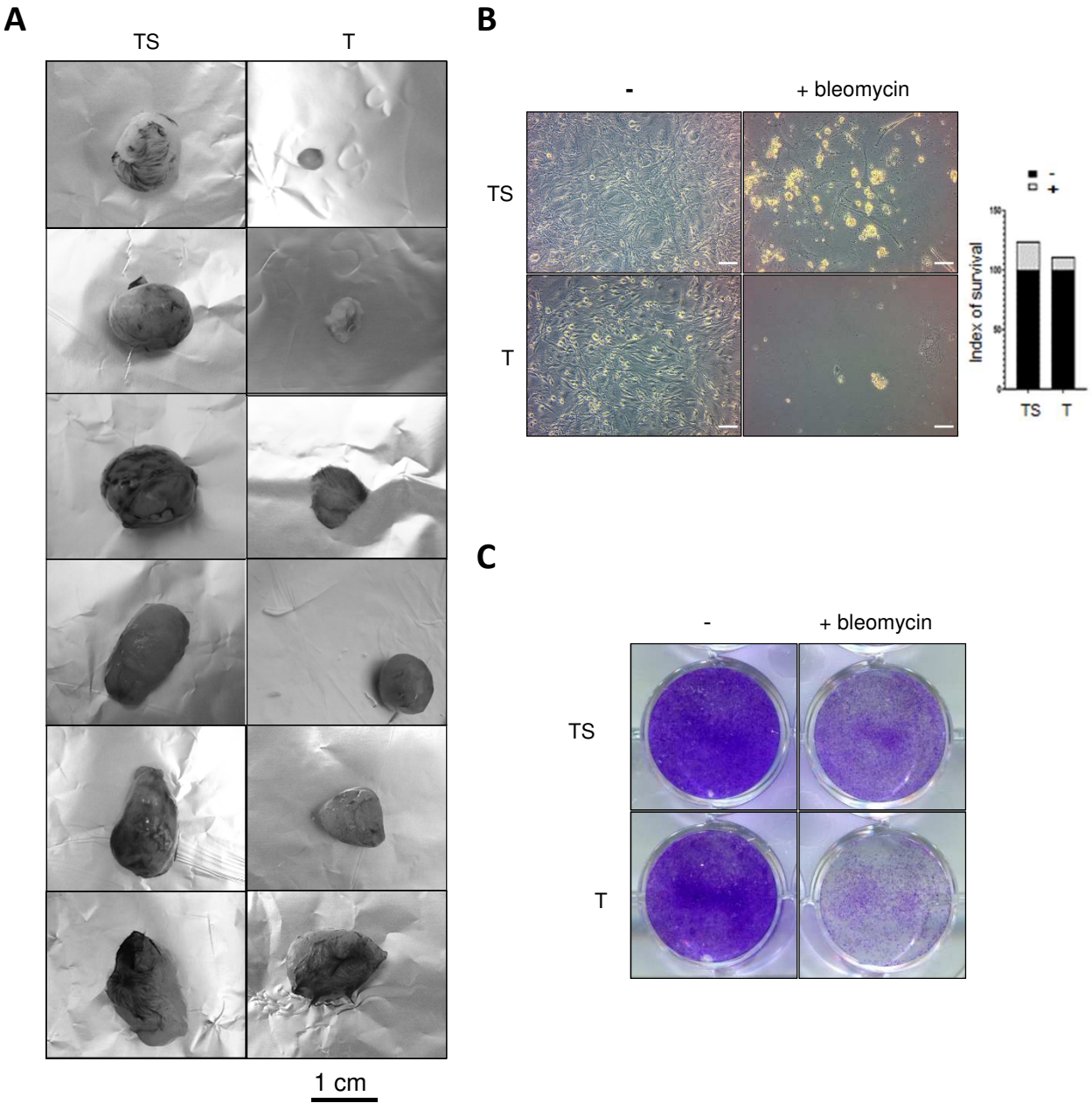

Suppl. Fig. 2 Transformed senescent (TS) cells are more tumorigenic and resistant to cell death. (A) After engrafting 5 million TS and T cells, mice were sacrificed after 13 days and tumors were photographed. **(B-C)** The day after seeding, TS and T cells were treated or not with 12 µg/mL bleomycin. **(B)** Five days later, images were acquired (scale bar= 100 µm) and **(C)** cells were fixed, and crystal violet stained.